Electron-beam lithography for micro and nano-optical applications

Daniel W. Wilson, Richard E. Muller, and Pierre M. Echternach
Jet Propulsion Laboratory
California Institute of Technology
Pasadena, California 91109

ABSTRACT

Direct-write electron-beam lithography has proven to be a powerful technique for fabricating a variety of micro- and nano-optical devices. Binary E-beam lithography is the workhorse technique for fabricating optical devices that require complicated precision nano-scale features. We describe a bi-layer resist system and virtual-mark height measurement for improving the reliability of fabricating binary patterns. Analog E-beam lithography is a newer technique that has found significant application in the fabrication of diffractive optical elements. We describe our techniques for fabricating analog surface-relief profiles in E-beam resist, including some discussion regarding overcoming the problems of resist heating and charging. We also describe a multiple-field-size exposure scheme for suppression of field-stitch induced ghost diffraction orders produced by blazed diffraction gratings on non-flat substrates.

Keywords: electron-beam lithography, nanostructure fabrication, diffractive optics, micro optics

1. INTRODUCTION

Electron beam (E-beam) lithography is a technology that enables much of the research on novel nanoscale optical devices. As E-beam lithography tools are improved, it becomes possible to expose smaller and more precise dose patterns. However, with this ability comes the need to understand and develop subsequent resist and substrate processing techniques so that the precision exposures are realized as precision device features. In this paper, our goal is to present some of our techniques for performing binary and analog E-beam lithography, including discussion of problems we encounter and some solutions for overcoming those problems. In Sec. II, we describe how we use a ZEP-on-PMMA bi-layer resist process for reliable lift-off fabrication, and how we use virtual-mark height measurement to compensate for wafer bow and tilt. In Sec. III, we review our techniques for analog surface-relief pattern fabrication, and discuss some techniques we have used to overcome resist heating and charging issues. We also describe a multiple-field-size exposure scheme for suppression of field-stitch induced ghost diffraction orders produced by blazed diffraction gratings on non-flat substrates.

2. BINARY LITHOGRAPHY TECHNIQUES

2.1 ZEP-on-PMMA bi-layer resist processing for lift-off fabrication

Lift-off processing is a common technique for fabricating fine features in thin-layered materials. For reliable results, the resist must have an undercut profile. This is typically achieved using a resist bi-layer with a bottom layer that is developed more quickly than the top (imaging) layer. As feature sizes decrease and pattern density increases, the undercut profile becomes difficult to achieve and resist collapse is a common problem. In our laboratory, we have found that a resist bi-layer of ZEP-520 (Zeon Chemicals L.P.)[1] on top of PMMA (950K molecular weight (MW), MicroChem Corp.) [2], gives more reliable results than the PMMA-on-copolymer or PMMA(high MW)-on-PMMA(low MW) bi-layer systems developed in MIBK. Typical exposure dose at 100kV (JEOL 9300FS E-beam lithography system) is 170 $\mu C/cm^2$ and development is performed in two steps: the top layer is developed in p-xylenes for 1 min and the bottom layer in MIBK:IPA 3:1 for 2 min. The ZEP/PMMA process combines the speed and high resolution of the ZEP layer with the ease of lift-off provided by the PMMA under-layer, in addition to the possibility of controlling the amount of overhang by timing of the second developing state. We have also successfully used this process as an etch mask. Cross-section SEM images were not available for this paper, but Fig. 1 shows a test pattern of 100 nm lines and spaces fabricated by lift-off of aluminum on silicon. Duty cycle control was good and smaller features should be possible.

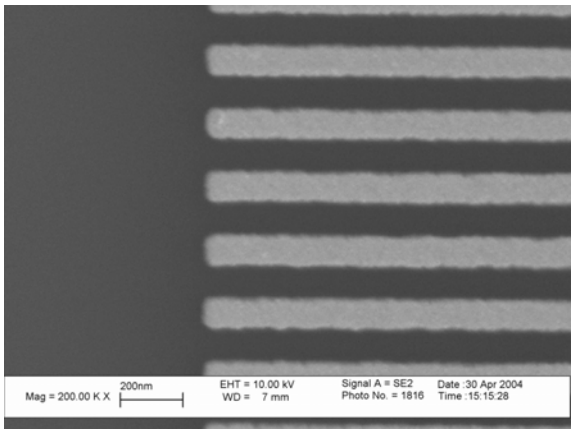

Figure 1. Test pattern of 100 nm lines and spaces of chrome on silicon fabricated by lift-off using a resist bi-layer of ZEP-520 on PMMA.

2.2 Virtual mark height measurement for reducing field-stitching in large patterns

A variety of optical components require the fabrication of precision binary gratings. These include distributed feedback lasers, phase masks for fabrication of fiber Bragg gratings, and integrated optical components for telecommunications and sensing applications. Advanced gratings incorporate phase-shifts to enhance the device performance, and thus such gratings cannot be fabricated by holographic lithography. All E-beam lithography systems have limited size writing "fields", and if the grating pattern is longer that the field size, the pattern is "stitched" together by moving the substrate stage. Exposure errors at the field-stitch boundaries and distortions within the field lead to periodic errors that cause device performance degradation in the form of laser mode side-lobes or "ghost" diffraction peaks. Regardless of how precise the E-beam deflector and stage system is, if the wafer height is not as expected or the wafer is bowed or tilted, such exposure errors will result. Such wafers (or pieces of wafers) are common in a research environment. One solution is to fabricate fiducial alignment marks within each writing field to allow the E-beam system to recalibrate for that location on the wafer. However, this is impossible or highly undesirable for many device structures. Recently, "virtual" mark detection was implemented on our JEOL 9300FS system allowing us to tell the tool where to make height measurements on the wafer. Those locations are specified at expose time in the script language that programs the exposure. The system will measure the height at the specified locations and perform dynamic corrections for focus, gain and rotation, interpolating the heights between the measured sites. This feature has made a significant improvement in the reliability of our long grating fabrication. As a test, we fabricated vernier patterns at the corners and at the center of fields distributed over a four-inch wafer that had over 100 µm of bow. For all fields, the field-stitch error was no greater than 20 nm.

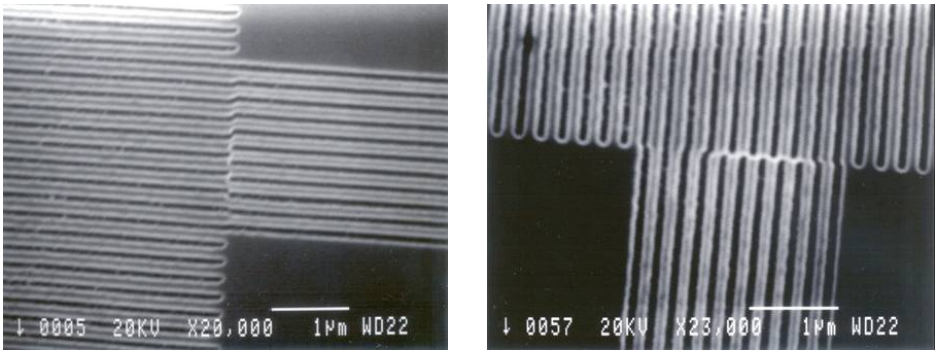

Figure 2. Vernier patterns used for measuring the field-stitching across a 4 inch bowed wafer. Left: near perfect alignment. Right: worst case (20 nm error).

3. ANALOG LITHOGRAPHY TECHNIQUES

Direct-write E-beam fabrication of analog-relief optics is attractive for rapid prototyping and low-volume precision production. Our techniques for fabricating analog surface-relief profiles in E-beam resist have been described previously,[4-7] but we will review them here in more detail to serve as a basis for further discussion.

2.1 Resist selection, processing, and calibration

When selecting a resist for analog-relief optics fabrication, the desirable characteristics are (1) high transmittance at the operating wavelength (not important for reflective optics), (2) low contrast for good depth control, and (3) good mechanical properties (adhesion, durability, thermal stability, etc.). Unfortunately, most resists are engineered for binary applications and hence exhibit high contrast with their recommended developers. In addition, thermal stability and durability are generally not a concern for binary lithography resists. For our optics, we have developed analog relief fabrication processes using polymethyl methacrylate (PMMA) and polymethylglutarimide (PMGI)[8].

PMMA is a very well known E-beam resist that has high resolution and very good optical properties. However, with a glass transition temperature of as low as 95°C, PMMA is restricted for use in low temperature applications. After spin coating, we bake PMMA in at 170°C for 30 min in a convection oven. Unfortunately, the recommended developer for PMMA, MIBK with IPA, gives high contrast leading to poor analog depth control. To achieve low contrast, we develop PMMA using pure acetone that is streamed (very low pressure) at the center of the spinning substrate by a timer-controlled dispense head. At the end of the prescribed development time, the stream is stopped and a nitrogen blow-off automatically turns on to dry the part immediately. Our typical total development time is approximately 15 seconds, but the development proceeds iteratively with optical and/or profile testing in between steps. Using this procedure, we can generally achieve less than 5-10% depth error. However, due to the spinning substrate, we observe radial falloff of the development rate, and this limits the substrate diameters to practically no larger than 2 inches.

As an alternative, PMGI resist has optical properties nearly as good as PMMA (in thin layers, at least) and much more attractive physical properties. With even better adhesion than PMMA and a glass transition temperature of 190°C, it can be used for more demanding applications. Furthermore, it is much easier to develop than PMMA because it has naturally low contrast when developed in standard alkaline developers. We typically perform a 10-20 minute bath development in AZ 300MIF developer (TMAH) diluted 1:1 with DI water (mild agitation).

Once a resist is selected, two main physical effects must be calibrated and compensated: (1) the nonlinear depth vs. dose sensitivity of the resist/developer combination, and (2) the proximity effect—exposure resulting from electrons back-scattered from underlying resist and the substrate. Figure 3 shows the broad-area depth, d vs. primary (E-beam delivered) dose, D_{prim} for PMMA and PMGI exposed at 100kV using our JEOL 9300FS E-beam system. The data are fit with a function $d = f(D_{prim})$ for pattern preparation. A simple exponential function fits the PMMA depth data almost perfectly, whereas a general (typically 3rd order) polynomial is required to fit the PMGI depth data. The proximity effect is more complicated to calibrate because the backscattering depends on the substrate material. The proximity effect is commonly described by a Gaussian model, and the dose point-spread function can be represented as

$$PSF(\mathbf{r}) = \delta(\mathbf{r}) + \frac{\eta}{\pi\alpha^2}\exp(-r^2/\alpha^2) \tag{1}$$

where η is the strength and α is the range. The incident beam can be represented as a delta function in Eq. (1) because the range of the proximity effect is large compared to the beam diameter and we are not concerned with correcting feature sizes on the order of the beam size. The total dose delivered to the resist is thus the primary (incident) dose convolved with the point-spread function. To characterize the proximity effect, we use a scanning probe microscope (SPM) to profile the edges of the same large area uniform exposures that are used to characterize the resist nonlinearity in Fig. 3(a). Figure 3(b) shows an SPM scan of PMMA exposed with 120 μC/cm^2 and developed for 15 seconds in pure acetone. The abrupt step is the edge of the primary dose pattern. The total dose delivered to the resist is the convolution of the primary dose pattern and the PSF. For the case of a broad area exposure, the dose at the edge can be derived analytically as the convolution of Eq. (1) with a step function to give

$$D_{tot}(x) = D_{prim}\left\{\mathrm{step}(x - x_{step}) + \frac{\eta}{2}\left[1 + \mathrm{erf}\left(\frac{x - x_{step}}{\alpha}\right)\right]\right\} \tag{2}$$

where D_{prim} is the value of the uniform primary dose. To fit the AFM profile and determine the proximity effect range and strength parameters, Eq. (2) is converted to depth using the nonlinear depth function from Fig. 1(a), with the dose axis scaled by (1+η) to account for the fact that for broad area exposures, $d = f\{D_{tot} = D_{prim}(1+\eta)\}$. Table 1 shows representative proximity effect parameters for different resist, substrate, and accelerating voltage combinations. For most substrates, the major effect in increasing the voltage from 50 to 100 kV is that the range increases by a factor between 3 and 4. In some cases, fitting was difficult and the strength parameter has significant uncertainty. To obtain a more accurate strength parameter, we typically expose an array of alternating step patterns that have been corrected with a range of strengths, and then choose the strength that gives the most accurate profile.

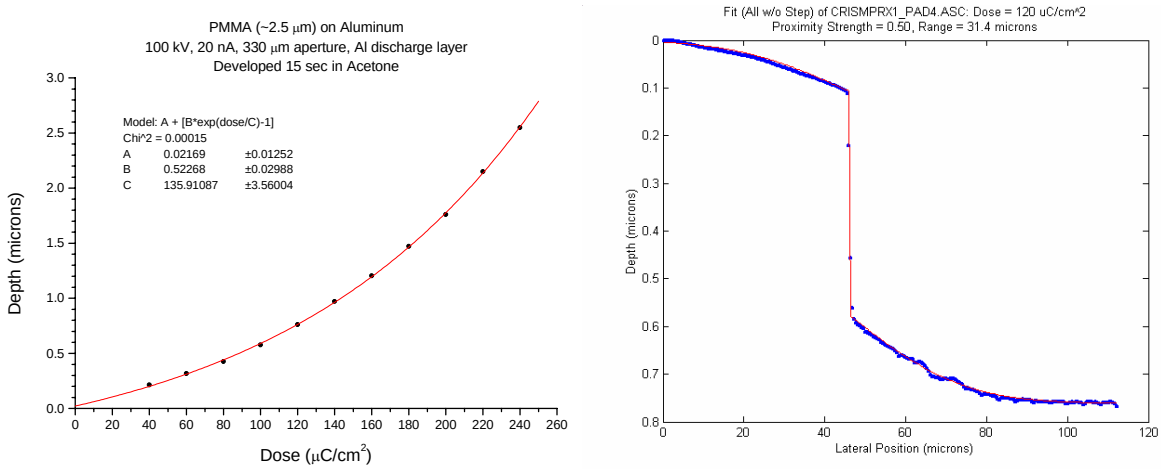

Figure 3. (a) Nonlinear depth vs. dose sensitivity of PMMA on aluminum (100 kV, 15 seconds acetone development). (b) scanning probe microscope profile of the edge of a uniform dose exposure of same PMMA as in (a). The solid line is a fit of Eq. (2) converted to depth, with strength η and range α as parameters.

Table 1. Proximity effect parameters

Substrate	**PMMA - 50 kV**		**PMMA - 100 kV**		**PMGI - 100 kV**	
	Strength, η	Range, α (μm)	Strength, η	Range, α (μm)	Strength, η	Range, α (μm)
Fused Silica	0.50	10.7	0.5	37	0.55	37.5
Aluminum	0.47	9.3	0.5	31	0.5	30
Silicon	0.48	10.6	0.55	41	0.55	41
GaAs	0.93	6.0	0.7	20	0.7	20

2.2 Pattern preparation

Once the nonlinear depth vs. dose response and the proximity effect parameters are known, a desired surface relief pattern can be converted to an E-beam dose pattern. To start, the desired depth profile is represented by an array of square or rectangular pixels. For blazed structures (gratings, diffractive lenses), the pixel size should be small compared to the local grating period to achieve low scattering and high efficiency. Each pixel will ultimately be exposed with the E-beam at the same accelerating voltage, but with a dwell time that is proportional to the desired depth. The pixel depths are converted to required *total* (incident + proximity) dose using the nonlinear depth function, $D_{tot}(x,y) = f^{-1}\{d(x,y)\}(1+\eta)$. The required primary dose for each pixel can then be determined by deconvolving Eq. (2) from the desired total dose pattern. In practice, this is performed using fast Fourier transform computations. Deconvolution of steps in the desired depth profile produces non-realizable negative doses. The solution is to recess the entire depth profile (typically 0.2 to 0.4 μm) until there are no doses less than some small positive value as described in

the next section. The final pattern preparation step is to convert the pattern of primary pixel doses into the native JEOL E-beam format using JPL in-house software.

2.3 Exposure parameters

Analog-relief lithography is exquisitely sensitive to exposure errors. Any overlap/underlap or other dose non-uniformity results in a surface-relief error that is typically visible even at low magnifications. When setting up E-beam system parameters, the following conditions must be satisfied to obtain a smooth surface: (1) the E-beam spot size must be greater than the spot spacing (the greater the overlap, the smoother the surface), (2) the pixel size should be an integer multiple of the spot spacing or "step", (3) on systems that use a sub-deflector, the sub-field size should be an integer multiple of the step size, and (4) the field size should be an integer multiple of the pixel size. When using the JEOL 9300FS, we do not find that these rules are restrictive when creating patterns. If a particular grating period is desired, we can generally find a combination of spot spacing and pixel size that comes close, and then fine pitch control can be used to stretch the writing pattern at expose time. Condition (1) actually requires the most attention when exposing analog relief patterns because such patterns usually contain at least a few pixels exposed at very low dose. Ideally the minimum dose would be zero (for minimum recess in the pattern as described above), but that would require the E-beam system to step infinitely fast. Each E-beam system has a spot scanner with a maximum frequency that limits the dwell time to a minimum value $t_{\min} = 1/f_{\max} = 1/25\text{MHz} = 40$ ns on our JEOL 9300FS. Hence for a given spot spacing, s (nm), and desired minimum dose D_{min} (μC/cm^2), the maximum allowed current is $I_{\max} = D_{\min} s^2 / t_{\min}$. In practice, we usually choose a minimum dose to be 40 μC/cm^2, so for a step size of 50 nm, the maximum current is 25 nA. The step size, and therefore the current, must be chosen so that the e-beam spot size is at least several times the step size to avoid roughness in the developed resist surface. Defocusing of the beam is possible, but it is important to calibrate the deflectors after defocusing to avoid field stitching errors.

2.4 Checkerboard exposure for minimizing resist heating

Most of our analog relief diffractive optic patterns are pixelized at a fine scale, and for cost effectiveness we prefer to expose them at high current (up to 60 nA). Recently, however, we have seen that when adjacent pixels are exposed sequentially, those pixel blocks are deeper than pixels that were exposed in isolation. Both types of exposures occur naturally in diffractive lenses. Near the x- and y-axes there are rows/columns of pixels of the same dose due to the circular Fresnel zones, whereas along the diagonals very rarely do two adjacent pixels have the same dose. Figure 4a shows a lens pattern exposed at 60 nA that shows a "cross" pattern through the central Fresnel zone. AFM inspection shows that the pixels in the cross are deeper than the rest of the lens (Fig. 4b). These observations naturally lead us to suspect that resist heating was causing an increase in the sensitivity. We verified this was the case by exposing the same pattern at significantly lower current (5 nA) in multiple passes and did not observe the cross pattern. However, writing at the lower current is not desirable due to the significant decrease in throughput. To avoid the problem and while still using high current exposure, we implemented a "checkerboard" writing scheme. Figure 4(c) illustrates the technique. The pixel pattern is split into two patterns "black" and "red" according to a checkerboard scheme. The "black" pattern is exposed first, and then the "red" pattern is exposed. Both patterns utilize many (typically hundreds) doses to achieve the desired analog surface relief, and in our software all the pixels of a given dose are exposed before the next dose. In this manner, no two adjacent pixels are ever exposed sequentially and the heating effect is minimized. In practice, our software creates a single pattern and a single dose table that implements this scheme, and it can easily be extended to higher order checkerboard patterns to further space the pixel exposures. To verify that this solved the problem, we wrote the same lens pattern at 60 nA with and without the checkerboard scheme. Fig. 4(e) shows that checkerboard-exposed lens showed no cross pattern.

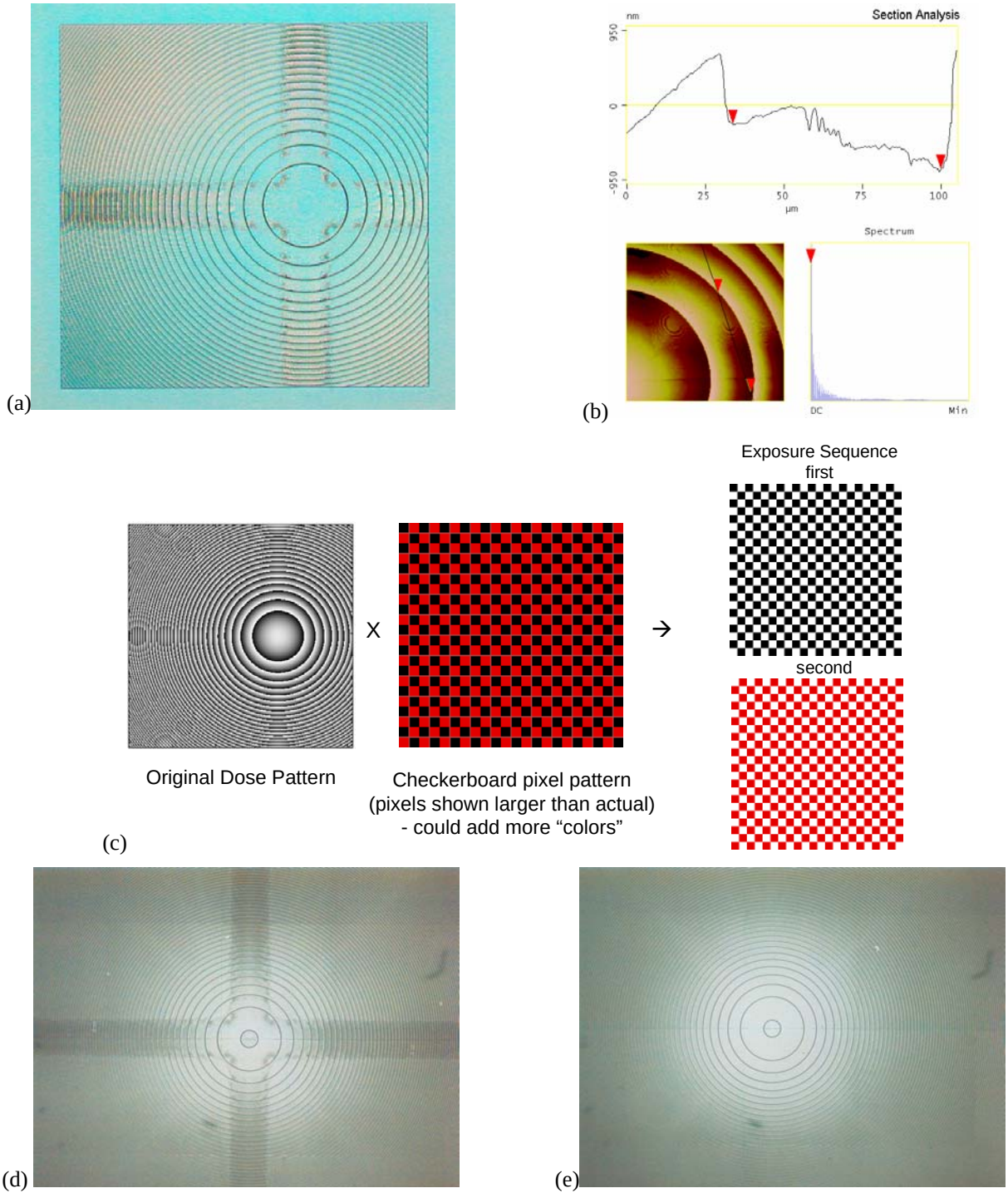

Figure 4. (a) "Cross" pattern of anomalous exposure depth in diffractive lens, (b) AFM scan showing cross region is deeper than desired, (c) checkerboard exposure scheme, (d) comparison lens exposed at 60 nA with standard exposure (no checkerboarding), (e) comparison lens exposed at 60 nA with checkerboard scheme.

2.5 Electron-beam system calibration for writing on convex and concave substrates

In recent years, there has been considerable interest in fabricating high-efficiency blazed gratings on convex and concave substrates[9-12] for imaging spectrometer applications. Our JEOL 9300FS has been specially modified by the manufacturer to allow writing on substrates with approximately 3.5 mm of height variation. This is termed the "sag" of the substrate, which for convex substrates is the dome to grating edge height. Accurate E-beam exposure on non-flat substrates is possible because the beam has significant depth of field (10's of µm) in its focus and pattern distortion parameters. The concept is straightforward—split the pattern up into 'zones' that correspond to substrate regions where the height changes by one depth-of-field as shown in Fig. 5. For spherical convex or concave substrates, these zones are annular in shape. The annular zone patterns are then exposed sequentially, adjusting the E-beam column settings for optimal writing at the mid-height of each zone. Great care must be exercised in determining the height-dependent column settings. We accomplish the calibration in the following manner. First, gold fiducial crosses are fabricated on a spherical convex substrate (lens) that has sag approximately equal to the maximum range of the E-beam system. This step is performed by focusing the E-beam at the center height and exposing as if the substrate were flat. Writing errors do occur, but the crosses require only low-resolution binary lithography. Next, the beam is manually focused on each cross to determine the focus setting as a function of height. The E-beam deflector calibration routine is run on each cross to determine functions for the x- and y-gain and x- and y-rotation settings for both the main- and sub-deflectors of the 9300FS. Once the height functions for the column settings are known, they can be used to determine parameters for a jobdeck HEIGHT command that is called before each zone pattern is exposed. This calibration procedure need only be performed after major column maintenance operations. For grating fabrication, a substrate having the same radius of curvature as the grating is height-mapped by focusing on silver or gold particles applied to the surface. This is necessary because the mounts for each grating job are unique and the absolute height can vary from the design. Finally, Figure 5 shows an optical micrograph showing the field (horizontal) and annular height-zone boundaries (curved). Note that the field boundary disappears near the middle of the annular zone, indicating that the deflector calibration was optimum at that height. This confirms that our deflector calibration and substrate mapping were accurate.

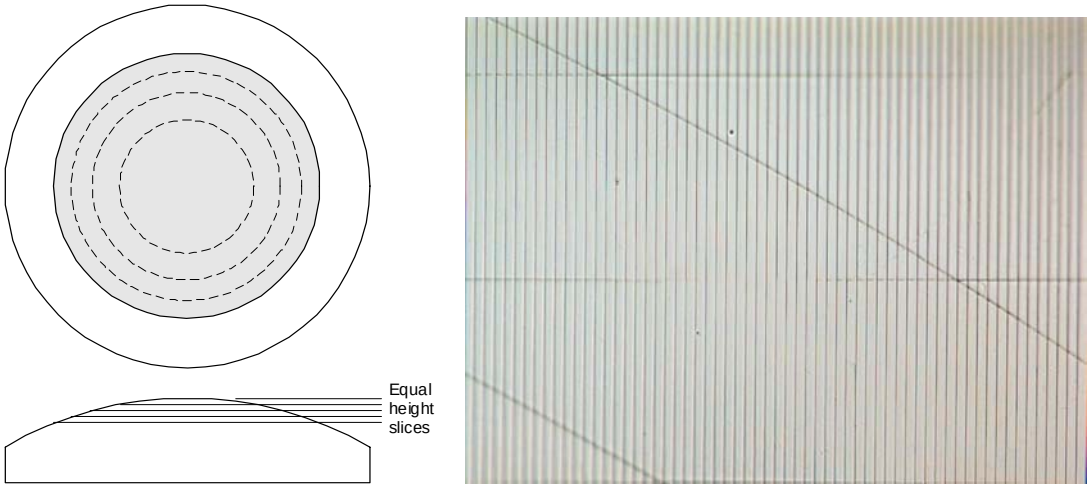

Figure 5. Pattern division scheme for E-beam exposure on non-flat substrates. Optical micrograph showing field- and annular-zone boundaries.

2.6 Multiple-field-size exposure for suppression of field-stitching ghosts

Field stitch errors are the dominant source of performance degradation in E-beam fabricated blazed gratings. Because all the fields are all of the same size, the stitching errors form another grating that has a period equal to the field size. Hence the light scattered from the field boundaries adds coherently to form ghost diffraction orders. To drastically reduce this effect, we split the overall grating pattern area into sub-areas and create patterns with different field sizes to fill each sub-area. For the case of convex or concave gratings, the sub-areas are naturally defined by the annular patterns that correspond to equal-height slices through the substrate surface. Hence each annulus is written with a different field size as shown in Fig 6.. Because the ghost order intensities are proportional to the square of the scattering amplitude, this reduces the ghosts by the square of the number of field sizes used. To test the technique, we fabricated two identical gratings: the first using a single field size everywhere, and the second using four different field sizes. Figure 6(c) shows measurement of the field. Measurement of the ghost order intensities from the second grating was impossible because they had effectively disappeared below the diffuse scattered background. The diffuse scattering in this grating is actually higher than we generally achieve due to some charging issues associated with the substrate.

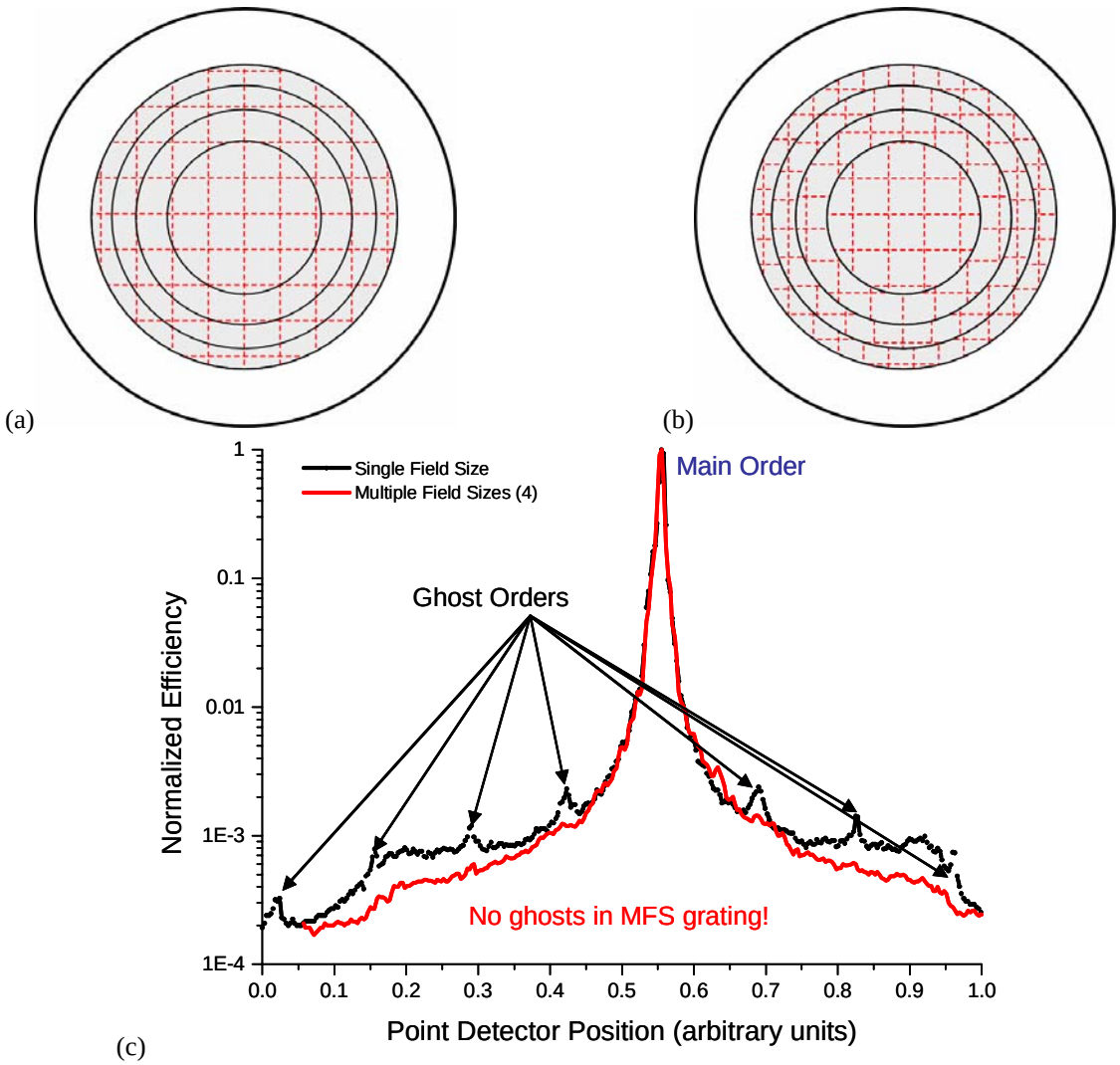

Figure 6. Comparison of single-field-size (SFS) and multiple-field-size (MFS) convex grating exposure schemes. (a) standard SFS writing scheme, (b) MFS writing scheme, (c) experimental comparison of a identical grating fabricated using single field size (dotted) and multiple (4) field sizes (solid).

4. SUMMARY

E-beam lithography is an extremely flexible technique for high-resolution binary- and analog-relief patterning. State-of-the art E-beam tools can deliver precision nanoscale dose patterns at high currents. The challenge is learning to avoid the physical and materials issues that can destroy the resolution and uniformity of the developed resist and ultimately the device material. We have presented a number of techniques that we have found useful for fabrication of optical devices in our laboratory.

ACKNOWLEDGEMENTS

We would like to thank Paul Maker for leading our group for 15 years, and for laying the foundation for much of the work discussed here. We would also like to thank Pantazis Mouroulis for many stimulating discussions and for pushing us to continue developing better techniques for fabricating convex and concave gratings. This research was carried out at the Jet Propulsion Laboratory, California Institute of Technology, under a contract with the National Aeronautics and Space Administration.

REFERENCES

1. http://www.zeonchemicals.com/productgrade.asp?id=218
2. http://www.microchem.com/products/pmma.htm
3. P. D. Maker, and R. E. Muller, “Phase holograms in poly methyl methacrylate,” J. Vac. Sci. Technol. B **10**, 2516-2519 (1992).
4. P. D. Maker and R. E. Muller, “Phase holograms in PMMA with proximity effect correction,” NASA CP-3227, 207-221 (1993).
5. M. Larsson, M. Ekberg, F. Nikolajeff, and S. Hård, P. D. Maker, and R. E. Muller, "Proximity-compensated kinoforms directly written by E-beam lithography," SPIE Proc. **CR49** (1993).
6. P. D. Maker, D. W. Wilson, and R. E. Muller, “Fabrication and performance of optical interconnect analog phase holograms made by E-beam lithography,” in Optoelectronic Interconnects and Packaging, R. T. Chen and P. S. Guilfoyle, eds., SPIE Proc. **CR62**, 415-430 (1996).
7. D. W. Wilson, P. D. Maker, and R. E. Muller, “Binary optic reflection grating for an imaging spectrometer," in Diffractive and Holographic Optics Technology III, SPIE Proc. **2689** (1996).
8. http://www.microchem.com/products/pmgi.htm
9. P. D. Maker, R. E. Muller, D. W. Wilson, and P. Mouroulis, “New convex grating types manufactured by electron beam lithography,” in Diffractive Optics and Micro-Optics **10**, OSA Technical Digest Series, 234-236 (1998).
10. P. Mouroulis, D. W. Wilson, P. D. Maker, and R. E. Muller, “Convex grating types for concentric imaging spectrometers,” *Appl. Optics* **37**, 7200-7208 (1998).
11. P. D. Maker, R. E. Muller, and D. W. Wilson, “Diffractive optical elements on non-flat substrates using electron beam lithography,” US Patent. No. 6,480,333, assigned to California Institute of Technology, Pasadena, CA (1998).
12. D. W. Wilson, P. D. Maker, R. E. Muller, P. Z. Mouroulis, and J. Backlund, “Recent advances in blazed grating fabrication by electron-beam lithography”, in *Current Developments in Lens Design and Optical Engineering IV*, Pantazis Z. Mouroulis, Warren J. Smith, and R. Barry Johnson, eds., pp. 115-126, Nov. 2003.